

The hidden physics in the dual-fermion approach - a special case of a non-local expansion scheme

Gang Li^{1,*}

¹ Institut für Theoretische Physik und Astrophysik, Universität Würzburg, 97074 Würzburg, Germany

In this work, we present a non-local expansion scheme to study correlated electron systems aiming at a better description of its spatial fluctuations at all length scales. Taking the non-local coupling as a perturbation to the local degrees of freedom, we show that the non-locality in the self-energy function can be efficiently constructed from the coupling between local charge fluctuations. It can provide one unified framework to incorporate non-locality to both ordered and disordered correlated many-body fermion systems. As the first application, we prove that the dual-fermion approach can be understood as a special case of this non-local expansion scheme. The scheme presented in this work is constructed without introducing any dual variable, in which the interacting nature and the correlated behaviors of the lattice fermions have a clear physics correspondence. Thus, in this special case, the equivalence of the dual-fermion approach to the non-local expansion scheme beautifully reveals the physics origin of the dual variables. We show that the non-interacting dual-fermion Green's function corresponds exactly to a non-local coupling of the lattice fermion renormalized by the local single-particle charge fluctuations, and the dual-fermion self-energy behaves as the one-particle fully irreducible components of the lattice Green's function. Not only limited to this specific example, the non-local expansion scheme presented in this work can also be applied to other problems depending on the choice of the local degrees of freedom.

PACS numbers: 71.10.Fd, 71.27.+a, 71.30.+h

I. INTRODUCTION

The Bloch's theorem [1] for electron states in crystals is based on their translational symmetry. These states are labeled by the quantum number k , which reflects their invariant behaviours under a translation by a Bravais lattice vector. However, the translational symmetry in a real solid is never perfect, which is not only because of its finite dimension, but also because of the presence of chemical potential/interaction disorders, lattice defects, impurities and phonons, etc. The finite dimension of a system may give rise to states which are sensitive to the surface but insensitive to the interior of the bulk. The chemical potential or interaction disorder localizes electron states in real space which can trigger a metal-insulator transition (also known as an Anderson transition [2]). In the ultracold atom system in optical lattices [3], though the lattice defects, impurities or phonons are absent, the spatial inhomogeneity is always present, as harmonic confinement potential introduces a spatially varying local density, which breaks translational symmetry of these cold atom systems. In addition, in systems with short-ranged magnetic correlations, the homogeneity can also be broken by the creation of ordered patterns in real space. When the concentration of disorder or magnetic patterns is small, the system can be treated approximately as if the translational symmetry were not broken, in this case the quantum number k can still be used to characterize the electron states. However, in the case with strong disorders, the translational symmetry

should be completely abandoned. Thus, it is important to have a unified theoretical framework to capture the effects of spatial inhomogeneity, especially in the presence of strong electronic correlations.

This problem represents a strong challenge to modern many-body theories. Due to the presence of the strong electronic correlation, approaches formulated from either weak-coupling or strong-coupling expansions, such as fluctuation exchange (FLEX) [4], random phase approximation (RPA), cumulant expansion [5, 6], strong-coupling expansion [7, 8], etc. are not adequate to handle the complete parameter range in interaction. Unbiased numerical approaches, such as exact-diagonalization and quantum Monte Carlo [9, 10], can treat the correlation effect precisely, but with the penalty on their finite cluster size, *i.e.* thermodynamic limit is not directly available in these approaches. Another class of many-body approaches, based on the dynamical mean-field theory (DMFT) [11], can fairly treat electronic correlation at arbitrary strength and contain the thermodynamic limit from its construction. It has been shown that, the DMFT can provide very important insights for several nonperturbative properties, such as the Mott-Hubbard transition. It also shows its great power in the study of correlated inhomogeneous systems. In the so-called real-space DMFT (R-DMFT) [12, 13], the correlated and disordered sites are treated as a group of Anderson impurities, which are embedded into a lattice system at the thermodynamic limit via the DMFT self-consistency. However, the DMFT is exact only in the infinite spatial dimension limit, where the character of correlation effect is purely local in space. For realistic systems at finite dimension, the DMFT downgrades to an approximation, which neglects the spatial fluctuation effect beyond the mean-field

* Correspondence and requests for materials should be addressed to: gangli@physik.uni-wuerzburg.de

level. For this reason, in the R-DMFT, disorder and correlation effect is treated locally. The spatial fluctuations of the complete system are determined by the coupling of the impurities within strong-coupling perturbation theory at leading order only (mean-field level). Generalizing an impurity to a cluster incorporates the short-ranged spatial fluctuations inside the cluster. Both, a reciprocal-space (dynamical cluster approximation, DCA [14–16]) and a real-space construction (cellular dynamical mean field theory, Cellular-DMFT [17]) have been suggested. These approaches improve results for $D = 1, 2, 3$, but they are no longer exact in the $D = \infty$ limit and the longer-ranged spatial fluctuations beyond the mean-field level, in these approaches, are still missing.

In this paper, we consider a correlated system without translational symmetry and aim at a better description of the spatial fluctuations at all length scale in the presence of strong electron-electron interaction. To this purpose, we generalize the strong-coupling expansion approach (cumulant expansion) to such a system and treat the non-local coupling as perturbations. The expansion of the non-local coupling can generate, order by order, the non-local spatial fluctuations from the coupling of the local charge fluctuations at different spatial locations. Depending on the choice of the local system, this scheme can either nicely go beyond the R-DMFT approximation to result in a non-local self-energy for correlated disordered systems or provide a quick cluster solver for the Cellular-DMFT. Not limited to these two specific applications, our scheme provides one unified framework to incorporate non-locality to a correlated many-body system with only moderate numerical cost.

II. NON-LOCAL EXPANSION

The translational symmetry of a homogeneous correlated system can be broken, for example, by disorders in chemical potential or interactions. But inhomogeneity in a real system can be much more general and have many different origins. The only assumption we make in this work is that the interaction shall be local. An example Hamiltonian looks like the following,

$$H = - \sum_{i,j} (c_{i\sigma}^\dagger \mathbf{t}_{ij} c_{j\sigma} + h.c.) - \sum_i \mu_i n_i + \sum_i U_i n_{i\uparrow} n_{i\downarrow}. \quad (1)$$

Here, the values of the chemical potential μ_i and the Coulomb repulsion U_i depend on their spatial coordinations, their different values in space give rise to the spatial inhomogeneity. \mathbf{t}_{ij} , in this equation, does not have to be restricted to only nearest neighbors. It can be quite general that to contain more hopping terms, or spatial anisotropy, etc. Eq. (1) represents one type of inhomogeneity that the systems could have. As we discussed before, there are many other ways to cause disorders to

the systems. Not losing generality, we discard the specific form of the Hamiltonian and only cast it into two parts for the convenience of the following discussions.

$$H = \sum_{i=1}^N H_i + H^{NL}. \quad (2)$$

H_i gathers every term that is locally related to site i . All other terms that carry non-locality are grouped into H^{NL} . The corresponding action can be written as

$$\begin{aligned} \mathcal{S} &= \int d\tau d\tau' \sum_{i,j} c_{i\sigma}^*(\tau) [\mathcal{G}^{-1}(\tau - \tau')]_{i,j} c_{j\sigma}(\tau') \\ &\quad + \sum_i \int d\tau U_i n_{i\uparrow}(\tau) n_{i\downarrow}(\tau) \\ &= \sum_{i=1}^N \mathcal{S}_i + \int d\tau d\tau' \sum_{i \neq j} c_{i\sigma}^*(\tau) [\mathcal{G}_\sigma^{-1}(\tau - \tau')]_{i,j} c_{j\sigma}(\tau') \\ &= \sum_{i=1}^N \mathcal{S}_i + T \sum_{i \neq j} \sum_\omega c_{i\omega\sigma}^* [\mathcal{G}_\sigma^{-1}(\omega)]_{ij} c_{j\omega\sigma} \end{aligned} \quad (3)$$

where $[\mathcal{G}(\omega)_\sigma^{-1}]_{ij}$ describes the dynamic coupling between states at different spacial locations. \mathcal{S}_i is the action that contains only the local degrees of freedom, in which $[\mathcal{G}_\sigma^{-1}(\omega)]_{ii}$ can have many different forms. For example, in the cellular-DMFT, $[\mathcal{G}(\omega)_\sigma^{-1}]_{ii} = -(\omega + \mu) + \Delta_{ii}(\omega)$, which is the local component of the inverse Weiss field. $[\mathcal{G}(\omega)_\sigma^{-1}]_{i \neq j}$ is the non-local hybridization function $\Delta_{i \neq j}(\omega)$. There are also many other possibilities of $[\mathcal{G}(\omega)_\sigma^{-1}]_{i \neq j}$. For the moment we keep $[\mathcal{G}(\omega)_\sigma^{-1}]_{i \neq j}$ as a general function that is purely non-local in space. At the end of this section, we will examine some specific forms of $[\mathcal{G}(\omega)_\sigma^{-1}]_{ij}$ to show that, actually, the formalism presented in this work can be nicely linked to some widely-known powerful methods, especially it can extend these local many-body approaches to partially include non-trivial spatial fluctuations. To be more precise, we refer the non-trivial spatial fluctuations to the spatial dependence in the self-energy function. If self-energy is only a local function, the corresponding spatial fluctuations are trivial.

A. diagram expansion

The general idea of the non-local expansion approach is very simple: we take the second term on the r.h.s. of Eq. (3) as a perturbation to the local action \mathcal{S}_i . By expanding this term, we will be able to determine the non-local dynamic quantity, such as the single-particle Green's function, from the local action \mathcal{S}_i . For simplicity, we take $[\mathcal{G}(\omega)_\sigma^{-1}]_{ij}$ as V_{ij}^ω and $\omega = (\omega, \sigma)$. With Eq. (3), the single-particle Green's function is calculated as

$$\begin{aligned}
G_{\alpha\beta}^{\omega} &= -\langle c_{\omega\alpha} c_{\omega\beta}^* \rangle = -\frac{1}{\mathcal{Z}} \int \mathcal{D}[c^*, c] \exp \left[-\sum_{i=1}^N \mathcal{S}[c_i^*, c_i] - T \sum_{i \neq j} \sum_{\omega'} c_{i\omega'}^* V_{ij}^{\omega'} c_{j\omega'} \right] c_{\omega\alpha} c_{\omega\beta}^* \\
&= -\frac{1}{\mathcal{Z}} \prod_{i=1}^N \int \mathcal{D}[c_i^*, c_i] e^{-\mathcal{S}_i[c_i^*, c_i]} \sum_{n=0}^{\infty} \frac{(-T)^n}{n!} \left[\sum_{i \neq j} \sum_{\omega'} c_{i\omega'}^* V_{ij}^{\omega'} c_{j\omega'} \right]^n c_{\alpha\omega} c_{\beta\omega}^*. \tag{4}
\end{aligned}$$

Here, α, β are two arbitrary spatial indices. \mathcal{Z} is the full partition function containing both local and non-local contributions.

$$\mathcal{Z} = \int \mathcal{D}[c^*, c] \exp \left[-\mathcal{S}_i[c_i^*, c_i] - T \sum_{i \neq j} \sum_{\omega'} c_{i\omega'}^* V_{ij}^{\omega'} c_{j\omega'} \right]. \tag{5}$$

\mathcal{Z} can be replaced by the local partition function $\mathcal{Z}_{loc} = \prod_{i=1}^N \mathcal{Z}_i$ when only the connected diagrams are considered in Eq. (4), as what we will do in this work. In a calculation with only the local \mathcal{S}_i , the single-particle Green's function one can get is the one with $\alpha = \beta$,

$$g_{\alpha}^{\omega} = -\prod_{i=1}^N \frac{1}{\mathcal{Z}_i} \int \mathcal{D}[c_i^*, c_i] \exp [-\mathcal{S}_i[c_i^*, c_i]] c_{\alpha\omega} c_{\alpha\omega}^*. \tag{6}$$

All terms for $\alpha \neq \beta$ vanish as the two operators, $c_{\omega\alpha}$ and $c_{\omega\beta}^*$, must pair in the above grassmann integral. With this in mind, we will proceed to evaluate the expansion in Eq. (4) order by order. Before proceeding, we want to note that Eq. (4) was more often evaluated by introducing a dual variable from the Hubbard-Stratonovich transformation [18, 19] on the non-local term. Here, we want to keep the present form of Eq. (4) and do not introduce any dual variable. At the end of this paper, we will compare our formalism to those obtained from the Hubbard-Stratonovich transformation to illuminate the physics hidden behind the introduction of the dual variables in those approaches.

The first term in the expansion of Eq. (4) is exactly the local Green's function as defined in Eq. (6). In the second term, α and β must be different as $i \neq j$. The only way to pair these operators is to set $i = \alpha$ and $\beta = j$, which gives rise to the first *non-local* correction to \mathcal{S}_i ,

$$G_{\alpha \neq \beta}^{\omega, (a)} = g_{\alpha}^{\omega} V_{\alpha\beta}^{\omega} g_{\beta}^{\omega}. \tag{7}$$

The graphical representation of this term is shown in Fig. 1(a). The wiggly line represents the non-local hybridization $V_{\alpha\beta}^{\omega}$ between the two spatial locations α and β . The solid line circling at each location represents the local Green's function computed from \mathcal{S}_i , as given in Eq. (6).

The third expansion term in Eq. (4) contains two topologically distinct diagrams. They correspond to the corrections of the non-local charge fluctuations to the local and non-local Green's functions, respectively. When $\alpha = \beta$, this term gives the first correction to the local Green's function g_{α}^{ω} , which is generated from the non-local charge fluctuations coupled with the local two-particle vertex. To see this, we need to examine the possible contractions of operators connecting to $c_{\alpha\omega} c_{\alpha\omega}^*$. In order to have a connected diagram, one has to link either $c_{j\omega'} c_{k\omega''}^*$ or $c_{i\omega'}^* c_{l\omega''}$ to $c_{\alpha\omega} c_{\alpha\omega}^*$ with the corresponding constraint $j = k = \alpha$ or $i = l = \alpha$. We notice that the interchange of indices i, j with k, l does not generate topologically new diagrams, thus, we can focus on only one of them and neglect the factor 1/2, *e.g.* $j = k = \alpha$.

$$\begin{aligned}
G_{\alpha=\beta}^{\omega, (b)} &= \frac{T^2}{\mathcal{Z}_{loc}} \sum_{i \neq j} \sum_{k \neq l} \sum_{\omega', \omega''} \int \mathcal{D}[c^*, c] e^{-\mathcal{S}_{loc}[c^*, c]} c_{l\omega''} c_{i\omega'}^* V_{i,j}^{\omega'} V_{k,l}^{\omega''} c_{j\omega'} c_{k\omega''}^* c_{\alpha\omega} c_{\alpha\omega}^* \delta_{\omega', \omega''} \delta_{i,l} \delta_{j,k} \\
&= T \sum_i \sum_{\omega'} \langle c_{i\omega''} c_{i\omega'}^* \rangle V_{i,\alpha}^{\omega'} V_{\alpha,i}^{\omega''} \langle c_{\alpha\omega'} c_{\alpha\omega}^* c_{\alpha\omega} c_{\alpha\omega}^* \rangle \delta_{\omega', \omega''}. \tag{8}
\end{aligned}$$

The last term in the above equation is the local four-point correlation function computed from \mathcal{S}_i .

$$\langle c_{\alpha\omega'} c_{\alpha\omega}^* c_{\alpha\omega} c_{\alpha\omega}^* \rangle = \langle c_{\alpha\omega'} c_{\alpha\omega}^* c_{\alpha\omega} c_{\alpha\omega}^* \rangle_c + \langle c_{\alpha\omega'} c_{\alpha\omega}^* \rangle \langle c_{\alpha\omega} c_{\alpha\omega}^* \rangle - \langle c_{\alpha\omega'} c_{\alpha\omega}^* \rangle \langle c_{\alpha\omega} c_{\alpha\omega}^* \rangle, \tag{9}$$

which contains both connected and disconnected parts. Eq. (8) corresponds to Fig. 1(b) if the connected four-point correlation function is used. The connected four-point correlation function is also called reducible two-particle vertex, which is graphically represented as the square in Fig. 1(b).

The disconnected part of $\langle c_{\alpha\omega'} c_{\alpha\omega}^* c_{\alpha\omega} c_{\alpha\omega}^* \rangle$ gives rise to a diagram topologically same as Fig. 1(c) but with $\alpha = \beta$. This is easier to see by first supposing $\alpha \neq \beta$ in the third order expansion, and releasing this constraint at the end of

the discussion,

$$\begin{aligned}
G_{\alpha \neq \beta}^{\omega, (c)} &= -\frac{T^2}{Z_{loc}} \sum_{i \neq j} \sum_{k \neq l} \sum_{\omega', \omega''} \int \mathcal{D}[c^*, c] e^{-\mathcal{S}_{loc}[c^*, c]} c_{\alpha \omega} c_{i \omega'}^* V_{i,j}^{\omega'} V_{k,l}^{\omega''} c_{j \omega'} c_{k \omega''}^* c_{l \omega''} c_{\beta \omega}^* \\
&= -\sum_j \langle c_{\alpha \omega} c_{i \omega'}^* \rangle V_{i,j}^{\omega'} V_{k,l}^{\omega''} \langle c_{j \omega'} c_{k \omega''}^* \rangle \langle c_{l \omega''} c_{\beta \omega}^* \rangle \delta_{i,\alpha} \delta_{j,k} \delta_{l,\beta} \delta_{\omega',\omega''} = g_{\alpha}^{\omega} \left(\sum_j V_{\alpha,j}^{\omega} g_j^{\omega} V_{j,\beta}^{\omega} \right) g_{\beta}^{\omega}. \quad (10)
\end{aligned}$$

Similar to Fig. 1(a), this diagram consists of only local single-particle charge fluctuations at different spatial locations which are connected by their dynamic hybridization. There will be more such diagrams in the higher order expansions of Eq. (4). These terms can be cast into a more compact form by renormalizing the hybridization as shown in Fig. 1(d). The dressed hybridization is simply found to be

$$\tilde{V}_{\alpha \beta} = [V^{-1} - g \mathbb{1}]_{\alpha \beta}^{-1}, \quad (11)$$

where $\mathbb{1}$ is an unit matrix. By replacing the single wiggly line with the double wiggly line, Fig. 1(a) becomes Fig. 1(e), which now incorporates all higher order diagrams similar as Fig. 1(c). With this substitution, we can now release the constraint of $\alpha \neq \beta$. Setting $\alpha = \beta$ in Fig. 1(c) does not violate any feynmann rule we used above, and it corresponds exactly to the diagram with disconnected four-point correlation function in Eq. (9). In fact, one can easily notice that only the crossing term, *i.e.* the last term of Eq. (9), leads to a connected diagram of $G_{\alpha \beta}^{\omega}$, which is same as what we derived in Eq. (10), but with $\alpha = \beta$.

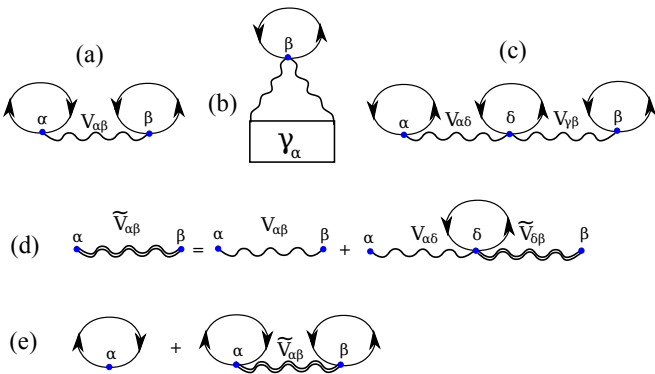


FIG. 1. A few lowest order Feynmann diagrams in the expansion of Eq. (4). (a), (b) and (c) correspond to the first three expansions. (d) The local single-particle charge fluctuations renormalize the non-local hybridization. With the renormalized hybridization $\tilde{V}_{\alpha \beta}$, diagrams similar to (a) and (c) now can be simply written as (e).

B. diagram resummation

The inclusion of all diagrams similar to Fig. 1(a) and (c) is of crucial importance to our non-local expansion scheme, which becomes clear in the following discussion. It has a very crucial implication in the non-interacting limit. With the dressed hybridization in Eq. (11), Fig. 1(a), (c) and all other similar diagrams can be cast into one simple diagram shown as Fig. 1(e). The single-particle Green's function evaluated from this diagram is given as:

$$G_{\alpha \beta}^{\omega, (e)} = g_{\alpha}^{\omega} \delta_{\alpha, \beta} + g_{\alpha}^{\omega} \tilde{V}_{\alpha \beta}^{\omega} g_{\beta}^{\omega}. \quad (12)$$

In the following, we will show that, with the dressed hybridization, Eq. (12) gives rise to $G_{\alpha \beta}^{0, \omega}$ exactly. This is a crucial condition to fulfill, as the non-interacting limit is an intuitive case to verify a diagrammatic approach. When interaction is switched off, *i.e.* $U = 0$, all reducible multi-particle susceptibilities vanish, thus, the only diagram we need to evaluate is Fig. 1(e).

$$G_{\alpha \beta}^{\omega} = g_{\alpha}^{0, \omega} \delta_{\alpha \beta} + g_{\alpha}^{0, \omega} [V^{-1} - g^{0, \omega} \mathbb{1}]_{\alpha \beta}^{-1} g_{\beta}^{0, \omega}. \quad (13)$$

In this equation, $g_{\alpha}^{0, \omega}$ is the local single-particle Green's function in the non-interacting limit, which shall be understood as $[[\mathcal{G}_{\sigma}(\omega)]_{\alpha \alpha}^{-1}]^{-1}$. It is different from the local Weiss field $\mathcal{G}_{\alpha \alpha}(\omega)$.

$$\begin{aligned}
G_{\alpha \beta}^{\omega} &= g_{\alpha}^{0, \omega} \delta_{\alpha \beta} + g_{\alpha}^{0, \omega} \left[\frac{V g^0}{\mathbb{1} - V g^0} \right]_{\alpha \beta} \\
&= g_{\alpha}^{0, \omega} \delta_{\alpha \beta} - g_{\alpha}^{0, \omega} \left[\mathbb{1} - \frac{1}{\mathbb{1} - V g^0} \right]_{\alpha \beta} \\
&= \left[\frac{1}{g^{0, -1} \mathbb{1} - V} \right]_{\alpha \beta} = \mathcal{G}_{\alpha \beta}^{\omega}. \quad (14)
\end{aligned}$$

Thus, the inclusion of local one-particle charge fluctuations at different spatial locations under the coupling of non-local hybridizations gives rise to the exact dynamics at all length scale in the non-interacting limit. At this point, it shall also be mentioned that, the current scheme can also correctly describe the strong coupling limit. In the strong coupling limit, the local dynamics becomes dominant, the expansion over $V_{\alpha \beta}$ becomes less important. \mathcal{S}_{loc} accounts for the major dynamics in that case.

In the intermediate coupling region, the diagrams with vertices become relevant. One example is Fig. 1(b), and

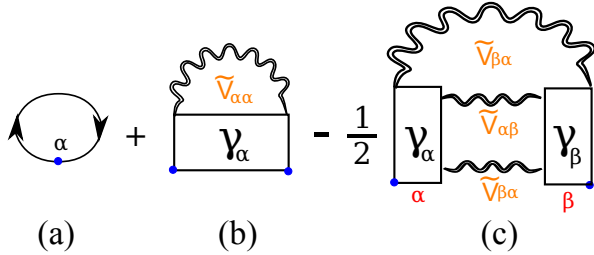


FIG. 2. The one-particle irreducible diagrams $\Lambda_{\alpha\beta}^\omega$ used for constructing the connected lattice Green's function in the non-local expansion scheme.

more similar diagrams appear in the higher order expansions of Eq. (4). In these diagrams, similar like the renormalization of the hybridization shown in Eq. (11), the higher order terms can be viewed as the dressed diagrams of lower order terms. Thus, we can cast these diagrams into a more compact form by using these lower-order diagrams as building blocks. Certainly, there are different ways to construct the higher-order diagrams from these building blocks, which corresponds to the different choices of the subset of the complete Feynmann diagrams in the expansion of Eq. (4). In this work, we consider the following resummation scheme whose physics meaning becomes clear in the end of this section.

$$G_{\alpha\beta}^\omega = \left[\frac{\Lambda^\omega}{1 - V^\omega \Lambda^\omega} \right]_{\alpha\beta}, \quad (15)$$

in which $\Lambda_{\alpha\beta}^\omega$ is the one-particle fully irreducible (1PI) diagrams taken as the construction blocks. Eq. (15) connects different 1PI diagrams of the single-particle propagator by the bare hybridization $V_{\alpha\beta}^\omega$. Intuitively, in Eq. (15), if we take the simplest 1PI diagram, which is $g_{\alpha\beta}^\omega \delta_{\alpha\beta}$, Eq. (12) is reproduced. It is obvious that, the more 1PI diagrams adopted in $\Lambda_{\alpha\beta}^\omega$, the better approximation we can get for $G_{\alpha\beta}^\omega$. As one will see in the next section, Eq. (15) can reproduce one advanced many-body approach, *i.e.* dual-fermion approach [20], when the local system is taken as the DMFT impurity.

For simplicity, in this work we consider the 1PI diagrams Fig. 2 for $\Lambda_{\alpha\beta}^\omega$. The first diagram in Fig. 2 is the local single particle propagator $g_{\alpha\beta}^\omega \delta_{\alpha\beta}$ calculated from the local \mathcal{S}_α . This diagram only gives rise to a mean-field description of the inter-site Green's function, which equally means that the self-energy computed from this diagram is still local. This can be seen by starting from Eq. (12) and repeating the derivation in Eq. (14) with $g_\alpha^{-1} = g_\alpha^{0,-1} - \Sigma_\alpha$. One can easily see that the lattice self-energy function $\Sigma_{\alpha\beta} = \Sigma_\alpha \delta_{\alpha\beta}$ is exactly the same as the local self-energy obtained from \mathcal{S}_α , *i.e.* no non-locality included in the self-energy. Fig. 2(b) corresponds to the diagrams with single-particle charge fluctuations coupled to a local two-particle scattering modes, which is obtained from Fig. 1(b) by replacing the hybridization with the dressed one, see Eq. (11). It is crucial to note that, though this diagram is local in space,

through Eq. (15), it generates spatial dependence of the *self-energy function* that is missing in Fig. 2(a). Fig. 2(c) consists of two connected four-point correlation functions $\gamma_\alpha^{\sigma_1\sigma_2;\sigma_3\sigma_4} = \langle c_{\alpha\omega_1} c_{\alpha\omega_2}^* c_{\alpha\omega_3} c_{\alpha\omega_4}^* \rangle_c$. In addition to the second diagram, it generates further non-local corrections to the lattice self-energy. The sum of the internal spin indices involved in this diagram can be more conveniently done by introducing $\gamma_\alpha^{c/s} = \gamma_\alpha^{\uparrow\uparrow\uparrow\uparrow} \pm \gamma_\alpha^{\uparrow\uparrow\downarrow\downarrow}$. $\Lambda_{\alpha\beta}^\omega$ is then found to be:

$$\begin{aligned} \Lambda_{\alpha\beta}^\omega &= g_{\alpha\beta}^\omega \delta_{\alpha\beta} - T \sum_2 \gamma_\alpha^{\sigma_1\sigma_2;\sigma_2\sigma_2} (11; 22) \tilde{V}_{\alpha\alpha}(\omega_2) \\ &\quad - \frac{T^2}{4} \sum_{234} \tilde{V}_{\beta\alpha}(\omega_2) \sum_{\delta=1}^N \tilde{V}_{\delta\alpha}(\omega_4) \tilde{V}_{\alpha\delta}(\omega_3) \\ &\quad [3\gamma_\alpha^s(12; 34)\gamma_\beta^s(43; 21) + \gamma_\alpha^c(12; 34)\gamma_\beta^c(43; 21)] \end{aligned} \quad (16)$$

Eq. (15) and Eq. (16) are the main results of our non-local expansion scheme. To construct non-locality from Eq. (16), only the local single-particle Green's function g_α^ω and the connected four-point correlation function $\gamma_\alpha^{c/s}(12; 34)$ are required. They are obtained from the solution of the local problem defined by \mathcal{S}_α , which can be easily accomplished with modern numerical algorithms. Thus, the total number of correlated sites N in these equations can be reasonable large to represent the thermodynamic limit. In this sense, both the short- and the long-range spatial fluctuations can be described by this formalism.

The computation flow of this new scheme is the following: one starts with the construction of the Weiss field $g_{\alpha\beta}^\omega$ and separates the local and non-local components as shown in Eq. (3). The local problem defined by the local component $g_{\alpha\alpha}^\omega$ and μ_α , U_α is then solved to get the local single-particle Green's function g_α^ω and the connected four-point correlation function $\gamma_\alpha^{c/s}(12; 34)$. Now Eq. (16) can be issued to compute the Green's functions $\Lambda_{\alpha\beta}^\omega$, which contain the non-trivial spatial fluctuations. With the new Green's function $G_{\alpha\beta}^\omega$ from Eq. (15), the self-energy $\Sigma_{\alpha\beta}^\omega$ can be calculated from Dyson equation, which contains both the local and non-local components and serves as the input for the next iteration of this calculation. The entire calculation shall stop only when $\Sigma_{\alpha\beta}^\omega$ does not change anymore.

The current scheme is formulated for the correlated system without translational symmetry. But it also applies to systems characterized by the quantum number k . As one unified scheme for both cases, here we also present the corresponding formula for the latter case. When the system is translationally invariant, only one impurity problem needs to be solved. The local impurity correlation functions g_α^ω and $\gamma_\alpha^{s/c}$ become completely site independent. After applying Fourier transform to Eq. (15) and Eq. (16), we have the following expressions for the lattice Green's function from the non-local expan-

sion scheme:

$$G_k^\omega = \Lambda_k^\omega / [1 - V_k^\omega \Lambda_k^\omega], \quad (17a)$$

$$\begin{aligned} \Lambda_k^\omega &= g^\omega - T \sum_2 \gamma_{\alpha}^{\sigma_1 \sigma_1; \sigma_2 \sigma_2} (11; 22) \tilde{V}_{\alpha \alpha} (\omega_2) \\ &\quad - \frac{T^2}{4N^2} \sum_{234} \sum_{k',q} \tilde{V}_{k+q} (\omega_2) \tilde{V}_{k'} (\omega_4) \tilde{V}_{k'+q} (\omega_3) \\ &\quad [3\gamma^s(12; 34)\gamma^s(43; 21) + \gamma^c(12; 34)\gamma^c(43; 21)]. \quad (17b) \end{aligned}$$

III. APPLICATION: NEW INSIGHTS INTO THE DUAL-FERMION APPROACH

The current scheme corresponds to the linked-cluster (or cumulant) expansion approach [6, 21, 22] if V_{ij} is simply taken as t_{ij} in Eq. (1). If the local system is taken as an DMFT impurity, this scheme is equivalent to the strong-coupling theory for interacting lattice models [8, 21]. Particularly, the diagram-resummation algorithm Eq. (15), corresponds to the [23, 24]. Furthermore, depending on the definition of the local problem, the non-local expansion scheme presented in this work can also be connected to and further extend some well-known local many-body approaches. As the first application, in this section, we will show that the dual-fermion approach exactly corresponds to one special case of the non-local expansion scheme for translational invariant system. From the current non-local expansion scheme, we want to explain the physics hidden behind the usage of the dual variables.

In Eq. (4), we have employed a direct expansion of V_{ij} and considered the expansion in orders. Now, we want to perform the same expansion by introducing a dual variable through the Hubbard-Stratonovich transformation. This is also known as a strong-coupling expansion of the Hubbard model [5, 25]. The main question we want to address in this section is that, by taking a different form of V_{ij} , we can prove that the dual-fermion approach [20] is equivalent to the current non-local expansion scheme with the diagram-resummation algorithm shown in Eq. (17).

The dual fermion approach is an elegant non-local extension of the DMFT, which was proposed for systems with translational symmetry. While there is obvious no obstacle for it to apply to inhomogeneous systems. One only needs to be careful with the breaking of translational symmetry and formulate it in coordination, instead of momentum space. Here, we would instead use Eq. (17) and prove that the current scheme can reproduce the dual-fermion approach for translational invariant system, if the local action is taken as the DMFT one.

According to the dual fermion approach, we add and

subtract a local dynamic function $\Delta_i(\omega)$ to Eq. (3),

$$\begin{aligned} S &= \sum_{i=1}^N \mathcal{S}_i + T \sum_{i,j} c_{i\omega}^* [\mathcal{G}_\sigma^{-1}(\omega)]_{ij} c_{j\omega} \\ &= \sum_{i=1}^N \mathcal{S}_i - T \sum_{k,\omega} c_{k\omega}^* (\Delta_\omega - \epsilon_k) c_{k\omega}, \quad (18) \end{aligned}$$

where \mathcal{S}_i is the local action of the impurity at the i th site, $\mathcal{S}_i = -(\omega + \mu) + \Delta_\omega + U n_{i\uparrow} n_{i\downarrow}$. Δ_ω , in principle, can be an arbitrary function. As shown in the dual fermion approach, diagrams for the dual fermion self-energy can be simplified if Δ_ω is taken as the hybridization function of the DMFT. In Eq. (18), V_k^ω is given as $-(\Delta_\omega - \epsilon_k)$, which contains both local and non-local components. One can still repeat the procedure shown in Sec. II to calculate the non-local single-particle Green's function. Due to the inclusion of the local component in V_k^ω , there are additional diagrams shall be considered. Fortunately, such diagrams, after the renormalization of V_k^ω , have actually been included in Fig. 2. Thus, the final expression of the single-particle Green's function from the non-local expansion scheme Eq. (17), also applies to the current case.

In the following, we want to show two important observations of the dual fermion approach. *First, we show that the physics origin of the non-interacting dual fermion propagator corresponds exactly to the renormalized hybridization \tilde{V}_k^ω .* To see this, we need to slightly modify the construction of the dual fermion approach. Different from the Hubbard-Stratonovich transformation generally employed in the dual-fermion approach [20], we set the coefficient of the mixing term between the original and the dual variables to be one. The full action in Eq. (18) becomes

$$\begin{aligned} \mathcal{S} = \mathcal{S}[c^*, c; f^*, f] &= \sum_{i=1}^N \mathcal{S}_i - \\ &\quad - T \sum_{k\omega} [f_{k\omega}^* c_{k\omega} + c_{k\omega}^* f_{k\omega} + \frac{f_{k\omega}^* f_{k\omega}}{\Delta_\omega - \epsilon_k}]. \quad (19) \end{aligned}$$

Then we proceed in the same way as the normal dual-fermion approach [20] does to get the exact relation between the lattice Green's function and the so-called dual-fermion Green's function:

$$G_{\alpha\beta}^\omega = (\Delta_\omega - \epsilon_k)^{-1} + (\Delta_\omega - \epsilon_k)^{-1} G_k^{d,\omega} (\Delta_\omega - \epsilon_k)^{-1}, \quad (20)$$

where $G_k^{d,\omega}$ is the single-particle propagator defined for the dual variables, whose non-interacting part is given as:

$$G_k^{d,0,\omega} = - [(\Delta_\omega - \epsilon_k)^{-1} + g^\omega]^{-1} = \tilde{V}_k^\omega. \quad (21)$$

From Eq. (21), one immediately understands that the non-interacting dual fermion propagator is not just a mathematical definition, it has clear physical correspondence. It corresponds to the dressed hybridization we

obtained in Eq. (11). As shown in the dual-fermion approach [20], the coarse graining of $G_k^{d,0,\omega}$ corresponds to the DMFT self-consistent equation.

$$-\sum_k \frac{1}{(\Delta_\omega - \epsilon_k)^{-1} + g^\omega} = \sum_k \tilde{V}_k^\omega = 0, \quad (22)$$

which indicates that the average of the non-local hybridization \tilde{V}_k^ω in momentum space is zero. This, from another perspective, reveals the local nature of the DMFT, *i.e.* the coarse graining effect of the non-local fluctuations vanishes in the single-particle level.

It also becomes transparent now that, in the non-interacting limit for the dual variables, the dual-fermion approach can give rise to the correct weak-coupling and the strong-coupling behaviors for a reason exactly the same as we discussed in Eq. (14). Furthermore, Eq. (21) also implies that the self-energy in the dual-fermion approach has the same set of Feynmann diagrams as the Green's function in our non-local expansion scheme, *i.e.* Fig. 2(b) and (c) are also the diagrams for the self-energy in the dual-fermion approach. As the dual-fermion self-energy is known to be analytic [20], the lattice Green's function of the non-local expansion scheme is, therefore, also an analytic function.

What is more subtle about the dual-fermion approach, which is the second important observation of this section, is that *it exactly the same as our non-local expansion scheme with the diagram-resummation algorithm due to Eq. (21)*. To prove this, we show the equivalence of Eq. (20) to Eq. (17). Starting from Eq. (20), after substituting $G_k^{d,\omega}$ with $G_k^{d,0,\omega}$ and the dual-fermion self-energy $\Sigma_k^{d,\omega}$, we have

$$\begin{aligned} G_k^\omega &= (\Delta_\omega - \epsilon_k)^{-1} + \frac{(\tilde{V}_k^{\omega,-1} - \Sigma_k^{d,\omega})^{-1}}{(\Delta_\omega - \epsilon_k)^2} \\ &= -\frac{1}{V_k^\omega} + \frac{(\tilde{V}_k^{\omega,-1} - \Sigma_k^{d,\omega})^{-1}}{(V_k^\omega)^2} \\ &= -\frac{1}{V_k^\omega} + \frac{1}{(V_k^\omega)^2} \frac{V_k^\omega / (1 - V_k^\omega g^\omega)}{1 - V_k^\omega \Sigma_k^{d,\omega} / (1 - V_k^\omega g^\omega)} \\ &= -\frac{1}{V_k^\omega} \left[1 - \frac{1}{1 - V_k^\omega (g^\omega + \Sigma_k^{d,\omega})} \right] \\ &= \frac{g^\omega + \Sigma_k^{d,\omega}}{1 - V_k^\omega (g^\omega + \Sigma_k^{d,\omega})}. \end{aligned} \quad (23)$$

In the above derivation, Eq. (11) and Eq. (21) have been employed. As we discussed before, the dual-fermion self-energy function employs the same Feynmann diagrams as shown in Fig. 2(b) and (c), *i.e.* $g^\omega + \Sigma_k^{d,\omega} = \Lambda_k^\omega$. Thus, Eq. (23) is exactly the same as Eq. (17). As no dual variable is involved in the construction of the non-local expansion scheme, the dynamics and physical correspondence of each term in Eq. (17) is clear. The equivalence of the dual-fermion and the non-local expansion scheme, thus, indicates that the interacting nature of the lattice

fermion in the dual-fermion approach is given exactly by Fig. 2, in which three different processes are taken as the most important contributions to the dynamics at all length scale. The first one reproduces the non-interacting limit through the non-local charge fluctuations; the non-local corrections to the lattice self-energy is generated by a single two-particle-scattering mode in Fig. 2(b) and the coupling of two two-particle-scattering processes in Fig. 2(c). All three processes, then, are coupled through Eq. (15) by the non-local hybridization V_k^ω . Such picture is less obvious in the dual-fermion approach.

Next, we will show that the lattice self-energy of the non-local expansion scheme as well as the dual-fermion approach, is one-particle fully irreducible. With Eq. (17), the lattice self-energy is found to be:

$$\begin{aligned} \Sigma_k^\omega &= \omega + \mu - \epsilon_k - 1/G_k^\omega \\ &= \omega + \mu - \epsilon_k - 1/(g^\omega + \Sigma_k^{d,\omega}) + V_k^\omega \\ &= \omega + \mu - \Delta_\omega - 1/(g^\omega + \Sigma_k^{d,\omega}). \end{aligned} \quad (24)$$

Given the DMFT Dyson equation $g^{\omega,-1} = \omega + \mu - \Delta_\omega - \Sigma_{loc}^\omega$, the above equation is then simplified as

$$\begin{aligned} \Sigma_k^\omega &= \Sigma_{loc}^\omega + 1/g^\omega - 1/(g^\omega + \Sigma_k^{d,\omega}) \\ &= \Sigma_{loc}^\omega + \frac{\Sigma_k^{d,\omega}}{g^\omega(g^\omega + \Sigma_k^{d,\omega})} \\ &= \Sigma_{loc}^\omega + \frac{\Sigma_k^{d,\omega}/(g^\omega)^2}{1 + g^\omega \Sigma_k^{d,\omega}/(g^\omega)^2}. \end{aligned} \quad (25)$$

The second term of the above equation generates diagrams consisting of multiple 1PI diagrams $\Sigma_k^{d,\omega}/(g^\omega)^2$ connected by single-particle propagator g^ω . Thus, it seems that Σ_k^ω from the non-local expansion scheme is one-particle reducible. However, as g^ω is a local function, it connects two one-particle irreducible diagrams $\Sigma_k^{d,\omega}/(g^\omega)^2$ locally. Thus, simply cutting g_i^ω does not result in the disconnection of the two $\Sigma_k^{d,\omega}/(g^\omega)^2$ at spatial location “ i ”. The lattice self-energy Σ_k^ω is, thus, one-particle irreducible. Note, a new 1PI generating functional with an expansion around the DMFT limit, recently, has also been proposed [26], which can directly generates the 1PI lattice self-energy diagrams.

In the last part of this section, we present a calculation for a correlated system with translational symmetry by using the non-local expansion scheme, which also represents a solution of the dual-fermion approach. In order to fully demonstrate the non-locality generated by these two approaches, we show, in Fig. 3, the lattice self-energy for a three dimensional cubic lattice with $U/t = 8$ along the high symmetry line R-M-X-Γ-R. The DMFT solutions have no momentum dependence, thus, they are straight lines in Fig. 3. The inclusion of non-locality, as shown in Eq. (17), generates dispersion in the real- and imaginary-part of the lattice self-energy around the DMFT solutions. Here, results are shown for two different temperatures. The lower temperature ($\beta t = 2.6$, see Fig. Fig3(b)) results display more pronounced momentum dependence of $\Sigma_k(i\omega_0)$ than the higher temperature

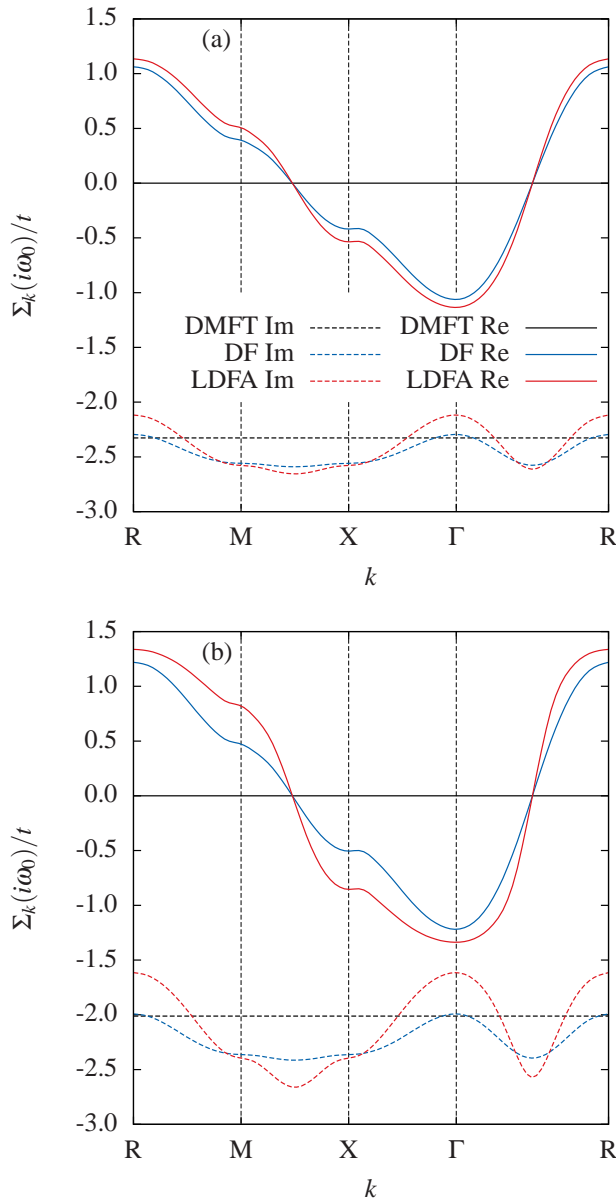


FIG. 3. The momentum dependence of the lattice self-energy in the non-local expansion scheme, as well as in the dual-fermion approach, for the single-band Hubbard model on a cubic lattice at (a) $\beta t = 2$, (b) $\beta t = 2.6$ and $U/t = 8$. The solid and dashed lines correspond to the real and imaginary parts of Σ_k^ω at the lowest Matsubara frequency. They agree well with the results from a calculation with the dynamical cluster approach, see ref. [27].

($\beta t = 2.0$, see Fig. 3(b)) ones. With the decrease of temperature, the spatial fluctuations are enhanced. In addition to the results from the dual-fermion approach and the non-local expansion scheme, Fig. 3 also shows the corresponding solution from Eq. (17) with a modified Λ_k^ω . In addition to the diagrams shown in Fig. 2, all ladder-type diagrams from both horizontal and vertical channels are included in this calculation. The additional scattering

processes included in the ladder diagrams yields a better inclusion of non-locality, thus, a more pronounced momentum dependence in $\Sigma_k(i\omega)$ can be observed. Without overhead thinking, one can immediately understand that the adoption of the ladder diagrams in Λ_k^ω in the non-local expansion scheme corresponds exactly to the ladder dual-fermion approach (LDFA) [28]. We want to note that the LDFA results shows surprisingly good agreement with the one from a dynamical cluster approach (DCA) calculations with a cluster of 100 sites (see Fig. 5 in Ref. [27]). Compared to the time-consuming large cluster DCA calculations, the present non-local expansion scheme, as well as the dual-fermion approach, is numerically much economical.

IV. CONCLUSIONS AND OUTLOOKS

In this paper, we proposed a non-local expansion scheme to study the correlated many-fermion systems. By separating the local and non-local degrees of freedom and assuming that the local system can be solved exactly (which, at least, can be achieved numerically), we can treat the non-local terms as a small perturbation to the local degrees of freedom. A non-local expansion around the solution of the local system can generate, order by order, the non-local corrections to the local solutions. This scheme can be widely applied to correlated systems with/without translational symmetry. Numerically, it is as economical as the DMFT, thus, a continuous momentum dependence in the self-energy function can be achieved easily in this scheme. As the first application, we have proven that the dual-fermion approach can be beautifully explained as one special case of the non-local expansion scheme presented in this work. When the local system is taken as the DMFT impurity and Λ_k^ω is approximated as the diagrams shown in Fig. 2 or ladder-type diagrams, the dual-fermion or the ladder dual-fermion approach is reproduced. Not limited to this case, in this section, we want to briefly outlook other possible applications of the non-local expansion scheme. More detailed discussions and the corresponding results will be presented elsewhere.

First, we want to show that the non-local expansion scheme can be used as a quick cluster solver for the Cellular-DMFT. In the Cellular-DMFT, the translational symmetry is naturally broken due to the different intra- and inter-cluster hopping amplitudes. Though in some special cases (for example in a 2×2 square cluster), the cluster momenta is still a good quantum number, we usually have to work with the situation that translational invariance is lost. Thus, Eq. (15) and (16) shall be used. In the Cellular-DMFT, the Weiss field contains the inter- and intra-cluster components. For a calculation with the non-local expansion scheme, in the first step we only need the diagonal component of the hybridization function $\Delta_{i,i}^\omega$, which we adopt to construct the local Weiss field $\mathcal{G}_i^\omega = -1/(\omega + \mu - \Delta_{i,i}^\omega)$, which is different

from the diagonal component of the Weiss field from the cellular-DMFT $\mathcal{G}_{i,i}^\omega = -[(\omega + \mu)\mathbb{1} - \Delta]_{i,i}^{-1}$. Thus, the separation of the local and non-local degrees of freedom looks like:

$$\mathcal{S} = \sum_{i=1}^N \mathcal{S}_i - T \sum_{i \neq j} \sum_{\omega} c_{i\omega\sigma}^* \Delta_{i,j}^\omega c_{j\omega\sigma}. \quad (26)$$

With the new \mathcal{G}_i^ω , an interacting impurity problem defined by \mathcal{S}_i is then solved to get the local self-energy Σ_i^ω and the local single-particle propagator g_i^ω , as well as the connected four-point correlation function $\gamma_i^{s/c}$. In the second step, the non-local expansion scheme Eq. (15) will be issued to calculate both the local and non-local components of the single-particle propagator g_{ij}^ω and the self-energy function $\Sigma_{i,j}^\omega$. The new Weiss field then can be calculated from $\Sigma_{i,j}^\omega$, which closes the Cellular-DMFT self-consistency loop. As one can immediately understand, the application of the non-local expansion scheme to the Cellular-DMFT equations can reduce the computational effort of solving a cluster problem to that of solving an impurity problem. Thus, a larger cluster calculation can be expected for the Cellular-DMFT with the non-local expansion scheme as cluster solver.

Second, the non-local expansion scheme can extend the R-DMFT to incorporate non-locality in the self-energy function. R-DMFT is widely used in the study of disordered correlated systems [29–33]. The disorders we considered here can be the different site energies ϵ_i and electronic correlations U_i , which are local in space. Thus, a DMFT-fashion calculation can be formulated. The R-DMFT iteration cycle begins with the calculation of the lattice Green's function,

$$G_{i,j}^\omega = \left[\frac{1}{(\omega + \mu)\mathbb{1} - \hat{t} - \hat{\epsilon} - \Sigma_i^\omega} \right]_{i,j}, \quad (27)$$

in which \hat{t} and $\hat{\epsilon}$ are of matrix forms. Matrix Σ^ω , in R-DMFT, is simplified to have only diagonal elements Σ_i^ω . For each site i , one defines a Weiss field $\mathcal{G}_i^\omega = [G_{i,i}^{\omega,-1} + \Sigma_i^\omega]^{-1} = (\omega + \mu) - \epsilon_i - \Delta_i^\omega$, from which the local Green's function g_i^ω and a new local self-energy Σ_i^ω can be calculated in the conventional DMFT. Normally, the R-DMFT closes the iteration cycle by substituting the new Σ_i^ω to Eq. (27). Now, with the non-local expansion scheme, a non-local self-energy can be obtained for the R-DMFT. Like in the dual-fermion approach, we separate the local and non-local degrees of freedom by adding and subtracting a local dynamic function Δ_i^ω to the denominator of Eq. (27). The non-local hybridization used for expansion in the non-local expansion scheme can be easily identified as $-(\Delta_i^\omega \mathbb{1} - \hat{t})$. With Eq. (15), a self-energy matrix with off-diagonal elements can be obtained, which generates the non-trivial spatial fluctuations to the R-DMFT. Here, it has to be noted that at each site i , g_i^ω and $\gamma_i^{s/c}$ take different values due to the site-dependent disorders. Thus, the single-particle charge fluctuations and the two-particle scattering modes differ at different sites. For this reason, the non-local expansion scheme essentially extends the non-local correlations of the R-DMFT from the one-particle to the two-particle level.

ACKNOWLEDGMENTS

We thank A.N. Rubtsov, H. Lee, H. Monien, H. Hafermann, A.I. Lichtenstein and W. Hanke for the fruitful collaborations on the dual-fermion approach. We thank A. Fleszar and K.S. Chen for reading the manuscript. We acknowledge the support from the DFG Grants No. Ha 1537/23-1 within the Forschergruppe FOR 1162 and SPP Ha 1537/24-2.

[1] F. Bloch, *Zeitschrift für Physik* **52**, 555 (1929).
[2] P. W. Anderson, *Phys. Rev.* **109**, 1492 (1958).
[3] I. Bloch, J. Dalibard, and W. Zwerger, *Rev. Mod. Phys.* **80**, 885 (2008).
[4] N. E. Bickers, D. J. Scalapino, and S. R. White, *Phys. Rev. Lett.* **62**, 961 (1989).
[5] S. K. Sarker, *Journal of Physics C: Solid State Physics* **21**, L667 (1988).
[6] W. Metzner, *Phys. Rev. B* **43**, 8549 (1991).
[7] N. DUPUIS and S. PAIRault, *International Journal of Modern Physics B* **14**, 2529 (2000).
[8] S. Pairault, D. Sénéchal, and A.-M. S. Tremblay, *Phys. Rev. Lett.* **80**, 5389 (1998).
[9] R. Blankenbecler, D. J. Scalapino, and R. L. Sugar, *Phys. Rev. D* **24**, 2278 (1981).
[10] D. J. Scalapino and R. L. Sugar, *Phys. Rev. B* **24**, 4295 (1981).
[11] A. Georges, G. Kotliar, W. Krauth, and M. J. Rozenberg, *Rev. Mod. Phys.* **68**, 13 (1996).
[12] R. W. Helmes, T. A. Costi, and A. Rosch, *Phys. Rev. Lett.* **100**, 056403 (2008).
[13] A. Katanin, *Journal of Physics A: Mathematical and Theoretical* **44**, 495004 (2011).
[14] T. Maier, M. Jarrell, T. Pruschke, and M. H. Hettler, *Rev. Mod. Phys.* **77**, 1027 (2005).
[15] M. H. Hettler, M. Mukherjee, M. Jarrell, and H. R. Krishnamurthy, *Phys. Rev. B* **61**, 12739 (2000).
[16] M. Jarrell, T. Maier, C. Huscroft, and S. Moukouri, *Phys. Rev. B* **64**, 195130 (2001).
[17] G. Kotliar, S. Y. Savrasov, G. Pálsson, and G. Biroli, *Phys. Rev. Lett.* **87**, 186401 (2001).
[18] J. Hubbard, *Phys. Rev. Lett.* **3**, 77 (1959).
[19] R. L. Stratovich, *Soviet Physics Doklady* **2**, 416 (1957).
[20] A. N. Rubtsov, M. I. Katsnelson, and A. I. Lichtenstein, *Phys. Rev. B* **77**, 033101 (2008).
[21] A. M. Shvaika, *Phys. Rev. B* **67**, 075101 (2003).
[22] E. Khatami, E. Perepelitsky, M. Rigol, and B. S. Shastry, *Phys. Rev. E* **89**, 063301 (2014).

- [23] M. Vladimir and V. Moskalenko, *Theoretical and Mathematical Physics* **82**, 301 (1990).
- [24] S. Vakaru, M. Vladimir, and V. Moskalenko, *Theoretical and Mathematical Physics* **85**, 1185 (1990).
- [25] S. Pairault, D. Snchal, and A.-M. Tremblay, *The European Physical Journal B - Condensed Matter and Complex Systems* **16**, 85 (2000).
- [26] G. Rohringer, A. Toschi, H. Hafermann, K. Held, V. I. Anisimov, and A. A. Katanin, *Phys. Rev. B* **88**, 115112 (2013).
- [27] P. Staar, T. Maier, and T. C. Schulthess, *Phys. Rev. B* **88**, 115101 (2013).
- [28] H. Hafermann, G. Li, A. N. Rubtsov, M. I. Katsnelson, A. I. Lichtenstein, and H. Monien, *Phys. Rev. Lett.* **102**, 206401 (2009).
- [29] V. Dobrosavljević and G. Kotliar, *Phys. Rev. Lett.* **78**, 3943 (1997).
- [30] Y. Song, R. Wortis, and W. A. Atkinson, *Phys. Rev. B* **77**, 054202 (2008).
- [31] D. Tanasković, V. Dobrosavljević, E. Abrahams, and G. Kotliar, *Phys. Rev. Lett.* **91**, 066603 (2003).
- [32] E. Miranda and V. Dobrosavljević, *Reports on Progress in Physics* **68**, 2337 (2005).
- [33] V. Dobrosavljević and E. Miranda, *Phys. Rev. Lett.* **94**, 187203 (2005).